Optics Communications 475 (2020) 126296

Contents lists available at ScienceDirect

Optics Communications

journal homepage: www.elsevier.com/locate/optcom

# Design and simulation of ultra-thin and high-efficiency silicon-based trichromatic PIN photodiode arrays for visible light communication

Dan Gao [a,b], Jun Zhang [b,c,d,*], Fan Wang [a], Jingqiu Liang [e], Weibiao Wang [e]

[a] MOE Key Laboratory of Disaster Forecast and Control in Engineering, School of Mechanics and Construction Engineering, Jinan University, Guangzhou 510632, China
[b] Department of Optoelectronic Engineering, Jinan University, Guangzhou, 510632, China
[c] Guangdong Provincial Key Laboratory of Optical Fiber Sensing and Communications, Jinan University, Guangzhou 510632, China
[d] Key Laboratory of Optoelectronic Information and Sensing Technologies of Guangdong Higher Education Institutes, Jinan University, Guangzhou 510632, China
[e] State Key Laboratory of Applied Optics, Changchun Institute of Optics, Fine Mechanics and Physics, Chinese Academy of Sciences, Changchun, Jilin, 130033, China

ARTICLE INFO

*Keywords:*
Array
Photodiode
Subwavelength structure
Nanostructure

ABSTRACT

Visible light communication offers abundant spectrum resources, which can alleviate the current shortage of wireless communication spectrum resources, and the security of the system is very reliable. In this study, a new photodiode (PD) array with micro-nano optical structure is designed and shown to effectively improve the absorption efficiency of PDs to blue, green, and red light. The absorption efficiency of blue, green, and red light at the central wavelength reached 96.8%, 97.5% and 98.6%, respectively, thus demonstrating the improved quantum efficiency of the device. Moreover, three color PDs are integrated into an ultra-thin silicon-on-insulator structure, increasing the integration and response speed of the device. The ultra-thin structure of the PD increases the response bandwidth up to the GHz level.

## 1. Introduction

Visible light communication (VLC) is becoming a popular means of wireless communication, as it can combine communication and illumination [1,2]. VLC uses illumination equipment instead of a traditional base station to transmit signals. The communication rate can reach tens to hundreds of megabits per second or even higher [3–5]. The receiving end can transmit high-speed wireless data as far as the light source can reach. The VLC system is very secure; as long as the light is blocked, the information will not leak. As the light is not disturbed by electromagnetic waves, it can be used freely in places affected by electromagnetic interference. It can also simultaneously provide lighting and communication, thereby improving energy utilization efficiency and meeting the energy-saving and green requirements of future communication systems. Owing to the rich spectrum resources of VLC, it can effectively alleviate the current shortage of wireless communication spectrum resources. A VLC system is mainly composed of signal modulation and coding, light source emission, transmission, and reception systems. The emission part of the VLC light source mainly consists of white light stimulated by a light-emitting diode (LED). White light is commonly produced either by mixing red, green, and blue (RGB) primary color LEDs or by using a blue LED to stimulate phosphor. The performance of the VLC receiver is one of the main parameters that determines the quality of a VLC system. As the sensitivity spectrum of silicon ranges from 380 to 1100 nm, the visible light detector of a VLC system consists mainly of silicon-based photodiodes (PDs). PIN silicon-based PDs and Avalanche Photo Diodes (APDs) are commonly used types. Researchers have proposed various structures to enhance the absorption of light by the detector to improve external quantum efficiency. These include silicon-on-insulator (SOI) lateral PIN PDs [6–10], SOI vertical PIN PDs [11], surface plasmon-enhanced PDs [12], metal–semiconductor–metal PDs [13], APDs [14–19], and transfer-printing flexible PDs [20]. Other approaches include forming a microstructure on the surface of the device using nanowires [21–23], photonics crystals [24,25], nano cones [26], or nano holes [27]. However, the above methods have disadvantages including low reliability, high operating voltages, low quantum efficiency, and high noise or response bands in the near infrared or ultraviolet regions. Regardless of the means by which the emitted light source is excited to produce white light, an increase in blue light efficiency is necessary. A white LED excited by RGB light can carry more channels, offering the possibility of wavelength division multiplexing, whereas the bandwidth of white light produced by blue-light-excited phosphor is limited by the relaxation time of the phosphor. In an RGB–white LED VLC system, when the RGB three-color LEDs carry signals, the detector needs to integrate three different wavelength detectors. The peak wavelength of the common silicon-based visible

* Corresponding author at: Department of Optoelectronic Engineering, Jinan University, Guangzhou, 510632, China.
*E-mail address:* 472969511@qq.com (J. Zhang).

https://doi.org/10.1016/j.optcom.2020.126296
Received 29 February 2020; Received in revised form 10 July 2020; Accepted 18 July 2020
Available online 22 July 2020
0030-4018/

light detectors on the market is about 600 nm. The absorption coefficients of silicon for blue and red light are very different. Therefore, the thickness of a red light detector is also very different from that of a blue light detector. The quantum efficiency of blue light is very low, generally less than 80%. In this study, a new PD structure is designed to integrate RGB trichromatic light PDs into a chip. Although the thickness of the absorption layer of the red light PD is larger than those of the blue and green light PDs, this paper proposes arranging the micro-nano optical structures in the intrinsic layer of the PD so as to ensure the absorption layer of the trichromatic light detector is ultra-thin and uniform. The response bandwidth of the PD is also improved by the ultra-thin structure, and the PDs are segmented by the micro optical electromechanical system technique to improve the response speed and integration of the device.

## 2. Design and simulation

### 2.1. Structural design

As the absorption depths of blue, green, and red light in silicon materials are different, there are two schemes that can meet the requirements of designing a trichromatic light-integrated PD in a chip with uniform thickness. One approach is to use the thickness of the short wavelength band PD in the design, and then use a special structure to reduce the transmissivity of the long wavelength band light; the other is to use the thickness of the long wavelength band PD, with a special structure to make the short wavelength light irradiate into the absorption layer as much as possible. For red light, when the absorption layer of the device is thick enough, the absorptivity of the device for red light will be greatly improved. However, when the thickness of the device is increased, the quantum efficiency of blue light will be reduced. This is because the absorption depth of blue light is shallow. Photons are absorbed on the device surface to produce photocarriers; however, as these simultaneously undergo recombination, they do not reach the absorption layer, so the quantum efficiency of blue light will be reduced. For blue light, when the non-depletion region of the device with vertical structure is thinner, blue light photons will enter the absorption layer. However, owing to the limitations of the technology, the high doping layer in the non-depletion region cannot be infinitely reduced, and a proportion of the blue light photons are always lost outside the depletion region; thus, the efficiency of blue light is always very low. In order to enhance the quantum efficiency of short wavelength photons, in 2006, Afzalian et al. proposed a lateral PD based on SOI film using Complementary Metal Oxide Semiconductor(CMOS) technology, and studied its photoelectric characteristics, quantum efficiency, and frequency characteristics. The quantum efficiency of the PIN PD was 56%–60% at the incident light wavelength of $\lambda = 400$ nm [6–10]. SOI technology effectively overcomes the shortcomings of bulk silicon devices with its unique all-media isolation structure, which can fully exploit the potential of silicon integrated circuit technology. Ultra-large scale integrated circuits are gradually being developed into mainstream technologies with high speed, low cost, high power consumption, high integration, and high reliability [28]. Detectors are moving in the direction of small size, portability, and high efficiency. In this study, we chose the first scheme to design the thickness of the photodiode, and we design an ultra-thin, high efficiency structure in which the three-color PDs are integrated into one chip. The specific structure of the device is shown in Fig. 1a. The device is an array with nine PDs integrated on the same chip. Each array has a two-dimensional periodic hole array with a micro-nano structure in its intrinsic layer. Fig. 1b shows a cross-sectional view of a single PD using a lateral PIN PD based on an SOI film.

### 2.2. Simulation

In order to reduce the reflection of short-wavelength light on the PD surface and the transmission of long-wavelength light through the PD, and to enhance the capture and absorption of photons, a micro-nano optical structure is included in the intrinsic layer of the lateral PIN PD based on SOI film. The micro-nano optical structure designed in the intrinsic layer of PD is a two-dimensional periodic hole array, which can be arranged in a cubic lattice or hexagonal lattice (as shown in Fig. 2). Usually, a fill factor is used to express the area percentage of air holes in the silicon upper surface, that is, $f=\pi d^2/4p^2$. The main parameters are the PD thickness $t$, and the period $p$, diameter $d$, and fill factor $f$ of the micro-nano optical structure. The optimal combination of parameters is determined by adjusting the values of the various parameters.

The absorptivity of the PDs can be calculated by subtracting the reflectivity ($R$) and transmissivity ($T$) components from the total intensity, that is, $A(\lambda)=1-R(\lambda)-T(\lambda)$. The absorption depth of visible light in silicon materials is related to the absorption coefficient. The absorption depth of blue light in silicon materials is about 0.5 μm, that of red light is from 2 μm to 10 μm, and that of green light is about 1.2 μm. The trichromatic photodiodes designed in this work are used to detect signals in the white light which is composed of red light (the red LED chip emission wavelength ranges from 615 to 650 nm, with a center wavelength of 620 nm), blue light (the blue LED chip emission wavelength ranges from 450 to 480 nm, with a center wavelength of 470 nm), and green light (the green LED chip emission wavelength ranges from 495 to 530 nm, with a center wavelength of 525 nm). The absorptivity of the lateral PIN PD can be simulated by the finite-difference time-domain method. FDTD Solutions software is produced by Canada Lumerical Solutions. FDTD is solved based on the vector 3-dimensional Maxwell equation, using the finite-difference time-domain method to mesh the space, and the time is calculated step by step, and the wide-band steady-state continuous wave results are obtained from the time-domain signal. The simulation conditions are shown in Table 1.

Considering the wavelength range of the PD and the absorption depth of the three-color light, in the micro-nano optical structure $p$ was set to 500 nm, $f$ was 50%, and $t$ was from 0.5 μm to 5 μm. The result of numerical FDTD simulation is shown in Fig. 3.

As shown in Fig. 3, when the wavelength range is 350–570 nm, the waveforms of the absorptivity, reflectivity, and transmissivity are relatively smooth. The absorptivity increases with increasing $t$, but when $t \geqslant 2$ μm, the absorptivity is almost unchanged with further increases in $t$. The transmissivity decreases as $t$ increases. When $t$ is 0.5 μm and 1 μm, the reflectivity fluctuates and the waveforms are similar. When $t \geqslant 2$ μm, the transmissivity is almost unchanged with increasing $t$. The reflectivity hardly changes with increasing $t$ except when $t$ is 0.5 μm. When the wavelength range is 570–800 nm, the waveforms of the absorptivity, reflectivity, and transmissivity change greatly. The absorptance still shows an upward trend with increasing $t$. When $t$ is 1 μm, a peak appears at a wavelength range of 672–683 nm, and the value is much larger than that at other thicknesses. It can be seen from the reflectivity curve that when $t$ is 1 μm, 2 μm, 3 μm, or 5 μm, the reflectivity decreases when the wavelength is between 500 nm and 600 nm. As the absorption depths of blue and green light are both less than 1 μm, and the absorption depth of red light is greater than 2 μm, the absorptivity, reflectivity, and transmissivity curves are different from others when the thickness is 0.5 μm or 1 μm. Thus, the incident light changes due to the air hole array in the PD intrinsic layer. The reflectivity and transmissivity are reduced by the various modes generated (this is explained in detail in the Discussion section). It can be seen from the absorptivity curve when $t$ is 1 μm that the micro-nano optical structure can improve the long wavelength absorptivity even when the thickness is small. When $t$ is 1 μm and $f$ is 50%, the absorptivity of PD at 400 nm, 450 nm, 500 nm, 550 nm, and 600 nm was simulated as shown in Fig. 4.

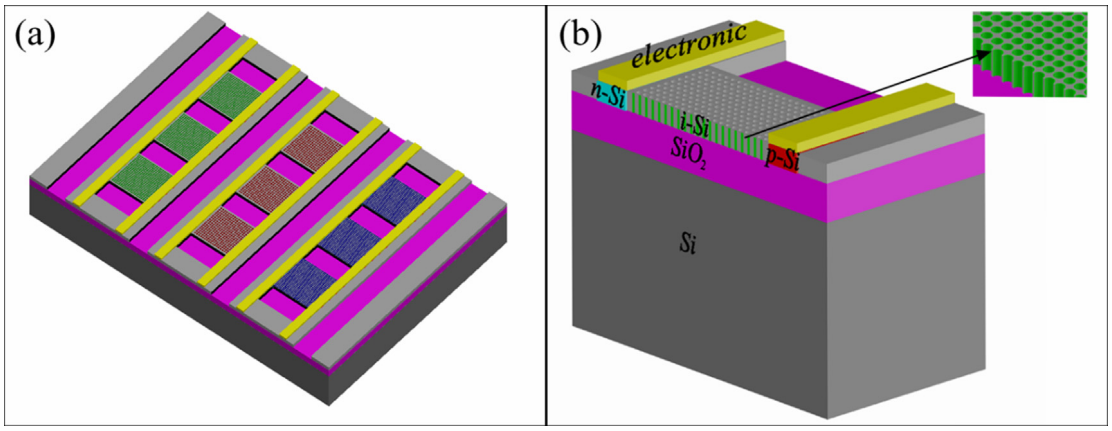


**Fig. 1.** (a) Structure of the ultra-thin lateral PIN trichromatic PD arrays with micro-nano optical holes in the intrinsic layer (i-layer). (b) Cross-sectional view of a single PD. Yellow, electronic; cyan, n-Si layer; red, p-Si layer; light gray, i-Si layer with air holes; carmine, $SiO_2$ layer; dark gray, Si substrate; green, air holes. . (For interpretation of the references to color in this figure legend, the reader is referred to the web version of this article.)

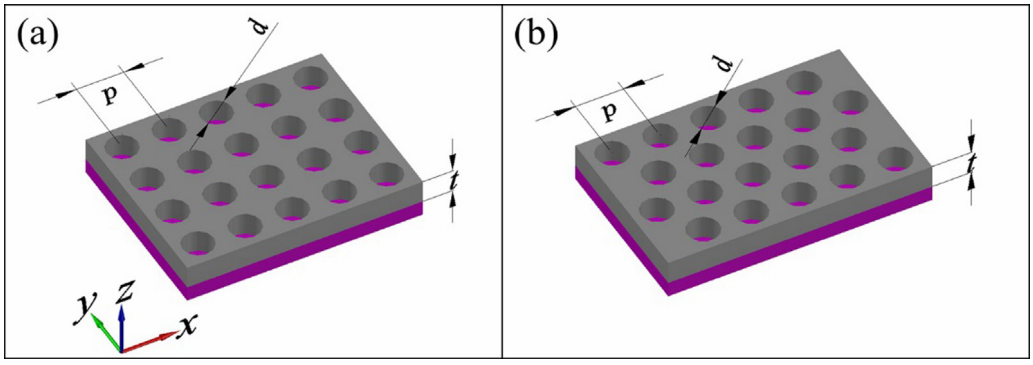


**Fig. 2.** Arrangement of micro-nano optical structures, where $t$ is the diode thickness, $p$ is the period, and d is the air hole diameter. (a) Cubic lattice array. (b) Hexagonal lattice array.

**Table 1**
The simulation conditions.

| Dimension | 3D |
|---|---|
| Si material properties | Complex dielectric permittivity |
| Mesh type | Auto non-uniform |
| $x$ and $y$ direction boundary condition | The periodic condition |
| $z$ direction boundary condition | The perfectly matched layer |
| Source shape | An incident vertical plane wave in -$z$ direction |

It can be seen from Fig. 4 that when the wavelength range is between 350 nm and 500 nm, the absorptivity, reflectivity, and transmissivity curves fluctuate less. With increasing $p$ of the micro-nano optical structure, the absorptivity decreases and the transmissivity increases. When the wavelength range is between 500 nm and 800 nm, the absorptivity, reflectivity, and transmissivity curves fluctuate greatly. With a change in $p$, the peak positions of each absorptivity curves also change. Notably, as shown in Fig. 4, the reflectivity plummets in special wavelength bands. When $p$ is 400 nm, the reflectivity curve drops sharply at $\lambda = 400$ nm, and the reflectivity is very low when the wavelength is between 400 nm and 500 nm. When $p$ is 450 nm, the reflectivity curve drops sharply at $\lambda = 450$ nm, and the reflectivity is very low when the wavelength is between 450 nm and 500 nm. When $p$ is 500 nm, the reflectivity curve drops sharply at $\lambda = 500$ nm, and the reflectivity is very low when the wavelength is between 500 nm and 600 nm. When $p$ is 550 nm, the reflectivity curve drops sharply at $\lambda = 550$ nm, and the reflectivity is very low when the wavelength is between 550 nm and 600 nm. However, when $p$ is 600 nm, the waveform of the reflectivity curve is very different from the others. The main reason for this result is that the absorption depth of the red light is greater than 2 μm, but the thickness of the PD is 1 μm. A rule can be developed based on the results shown in Fig. 4: when the wavelength is less than 600 nm, adjusting the period of the micro-nano optical structure can reduce the reflectivity of the PDs.

Fig. 5 shows the absorbance changes of the three colors when $p$ is 550 nm, $t$ is 1 μm, and $f$ is variable.

As shown in Fig. 5, when the fill factor changes, the absorptivity curve fluctuates greatly. When the wavelength is less than 600 nm, the waveform of the reflectivity curves of the four groups with different fill factors are similar. As $f$ decreases, the reflectance increases and the peak position moves toward the red light. When $f$ is 50% or 60%, the reflectivity still decreases at 550 nm. Fig. 6 shows a comparison of the absorptivity of the cubic lattice and the hexagonal lattice structure in the PD intrinsic layer and no structure on the PD surface when $p$ is 450 nm, $f$ is 50%, and $t$ is 1 μm. The absorptivity of the PD intrinsic layer with the micro-nano optical structure is much higher than that of the surface without a structure. This shows that the micro-nano optical structure can weaken the reflection and transmission of light.

As the absorption depths of blue and green light are less than 1 μm, and the absorption depth of red light is much greater, the thickness of the PD designed in this work was 1 μm. By adjusting the period and the fill factor, the absorptivity of the trichromatic light was improved. As

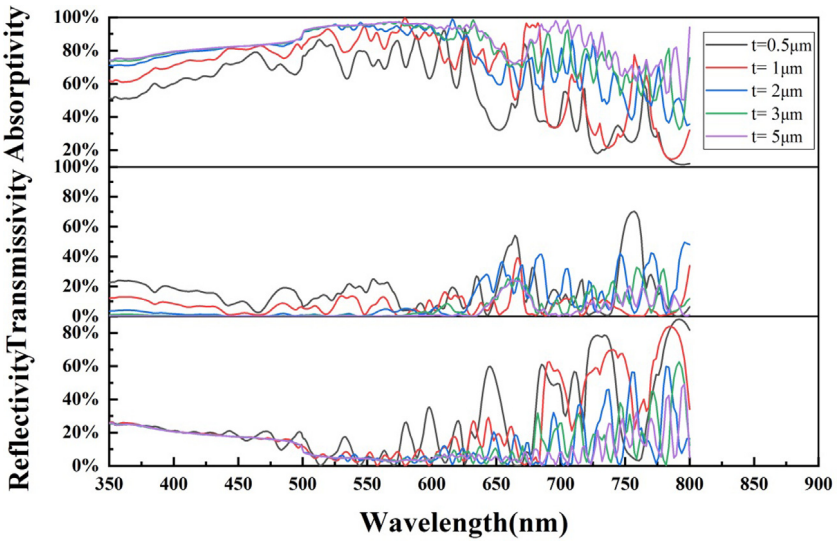


**Fig. 3.** Absorption, reflection and transmission spectra of micro-nano hole arrays with period $p = 500$ nm and fill factor $f$=50%. The black solid line represents the PD thickness $t = 0.5$ μm, the red line $t = 1$ μm, the blue line $t = 2$ μm, the green line $t = 3$ μm, and the purple line $t = 5$ μm. . (For interpretation of the references to color in this figure legend, the reader is referred to the web version of this article.)

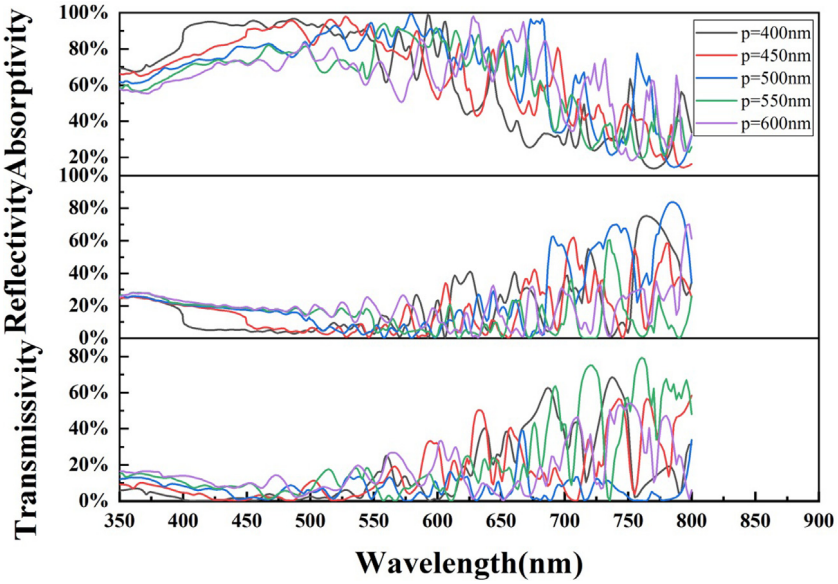


**Fig. 4.** Absorption, reflection, and transmission spectra of micro-nano holes arrays with thickness $t = 1$ μm and fill factor $f$=50%. The black solid line represents the micro-nano holes with period $p = 400$ nm, the red line $p = 450$ nm, the blue line $p = 500$ nm, the green line $p = 550$ nm, and the purple line $p = 600$ nm. . (For interpretation of the references to color in this figure legend, the reader is referred to the web version of this article.)

shown in Figs. 4 and 5, the $p$ and $f$ values of the micro-nano optical structure have a great influence on the absorption of light; a change in $f$ affects the position of the absorption peak, which is red-shifted or blue-shifted, whereas a change in $p$ affects the position of the decreasing reflectivity.

Fig. 7 shows the absorptivity, reflectivity, and transmissivity of the blue light PD. In the micro-nano optical structure, $p$ is 400 nm, $t$ is 1 μm, and $f$ is 60%. The absorptivity of the blue light LED chip at the center wavelength $\lambda$ of 470 nm reaches 96.8%. When the wavelength $\lambda$ is in the range 450–480 nm, the absorptivity is greater than 94%.

Fig. 8 shows the absorptivity, reflectivity, and transmissivity of the green light PD. In the optimal micro-nano structure, $p$ is 450 nm, $t$ is 1 μm, and $f$ is 55%. The absorptivity of the green light LED chip at the center wavelength $\lambda$ of 525 nm reaches 97.5%. When the wavelength $\lambda$ is in the range 495–530 nm, the absorptivity is greater than 92%.

Fig. 9 shows the absorptivity, reflectivity, and transmissivity of red PD. In the optimal micro-nano structure, $p$ is 550 nm, $t$ is 1 μm, and $f$ is 48%. The absorptivity of the red light LED chip at the center wavelength $\lambda$ of 620 nm reaches 98.6%. When the wavelength $\lambda$ is in the range 615–650 nm, the absorptivity is greater than 61%.

### 2.3. Discussion

A micro-nano optical structure was designed in the intrinsic layer of the trichromatic PD array. When the light is incident on the surface of the PD, it is also incident into the micro-nano holes, so that the illumination area of the incident light is increased. The air on the surface of the PD, the bulk silicon with holes, and the $SiO_2$ layer in the SOI structure constitute a fiber-like structure; thus, a total reflection process occurs in the silicon after the light was incident. The two-dimensional air holes are periodically distributed in the silicon to form a uniform Bragg grating, so that the light is coupled inside.

There are several modes for the frequencies in the visible spectrum, which contribute to energy transport and absorption. The degenerate

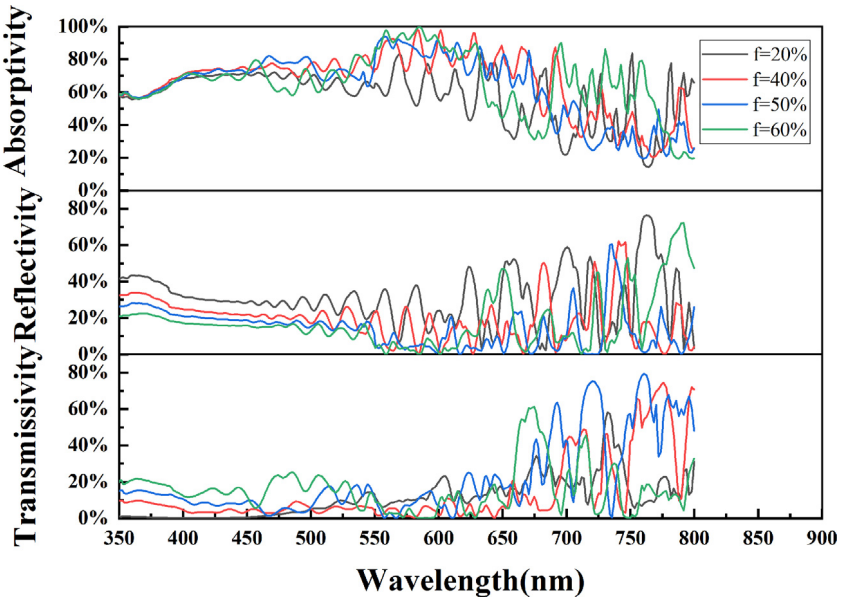


**Fig. 5.** Absorption, reflection and transmission spectra of micro-nano holes arrays with the thickness $t = 1$ μm and the period $p = 550$ nm. The black solid line represents the PD fill factor $f$=20%, the red line $f$=40%, the blue line $f$=50%, the green line $f$=60%. . (For interpretation of the references to color in this figure legend, the reader is referred to the web version of this article.)

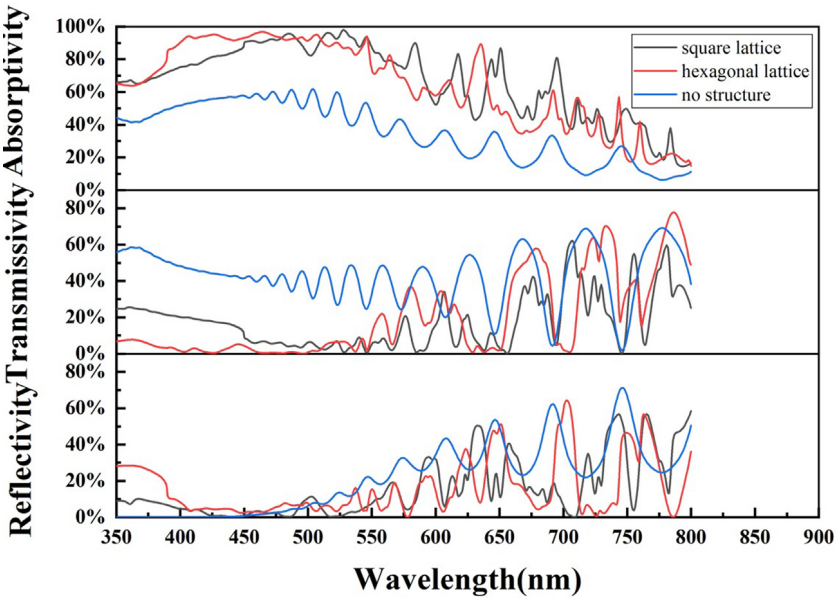


**Fig. 6.** Absorption, reflection, and transmission spectra of the PD. Black and red lines represent the micro-nano optical structures on the surface of silicon PDs, which are arranged cubic lattice and hexagonal lattice, respectively. The period $p$ of the optical micro-nano structure is 450 nm, the fill factor $f$ is 50%, and the PD thickness $t$ is 1 μm. The blue line represents the surface of the silicon PDs with no structure. . (For interpretation of the references to color in this figure legend, the reader is referred to the web version of this article.)

fundamental Bloch modes, guided resonance modes, and channeling Bloch modes are the main types for an incident plane wave in nano hole arrays [29,30]. The mode of incident light in the micro-nano structure may be a single type or a combination of multiple types. A steep waveform indicates guided mode resonance. If the waveform is relatively smooth, a fundamental mode or channeling mode is generated.

As shown in the reflectivity curves in Figs. 3–5, the reflectivity decreased sharply at $\lambda \approx$ p, mainly owing to the dominant channeling mode. The trough width of the reflectivity is related to the thickness of the PD and the period of the micro-nano optical structure. As shown in Figs. 3–9, the end position of the reflectivity trough was at $\lambda \approx 0.7/\alpha$, where $\alpha$ is the absorption coefficient of bulk silicon. When $t$ was 0.5 μm (Fig. 3), the reflectivity is different from the other cases because the fundamental mode and the guided resonance mode were the main modes in the whole spectrum. The thicknesses of the PDs used in this work were designed to be 1 μm, so the end wavelength of the reflectivity trough was about 600 nm. As shown in Fig. 4, the end wavelength of the reflectivity trough was very close to the value of the period when the period was 600 nm, so there was no reflectivity trough in the waveform. When the fill factor was 20% or 40% (Fig. 5), the diameter of the air holes was very small, the fundamental mode and the guided resonance mode simultaneously exist and the guided resonance mode is the main mode which leads to the waveform sharply, so the waveform was different from the others. Effectively reducing the reflectivity on the surface of the PD and the transmissivity on the bottom of the PD will greatly increase the absorptivity of the device.

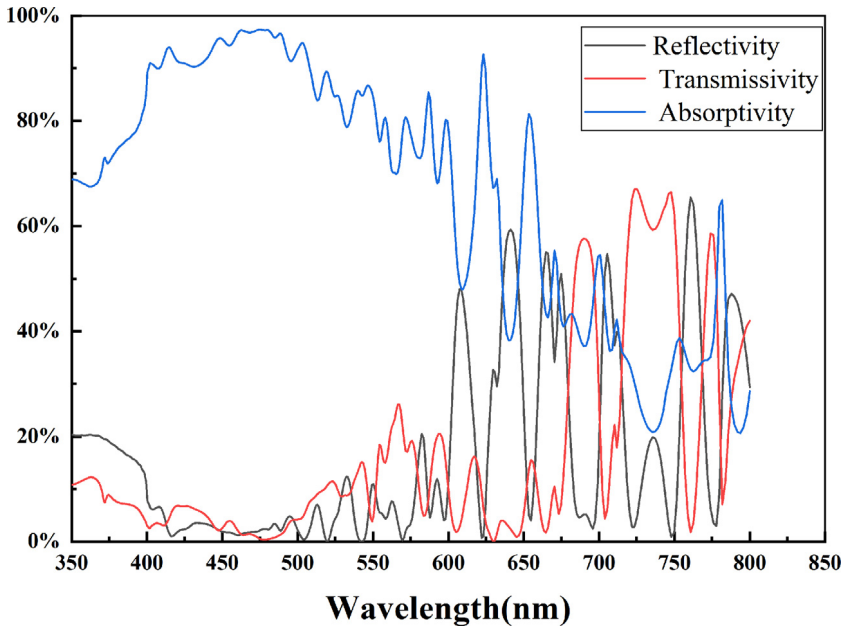


**Fig. 7.** Absorption, reflection, and transmission spectra of the blue light PD. Black cure shows absorptivity, red cure shows transmissivity, blue cure shows reflectivity. . (For interpretation of the references to color in this figure legend, the reader is referred to the web version of this article.)

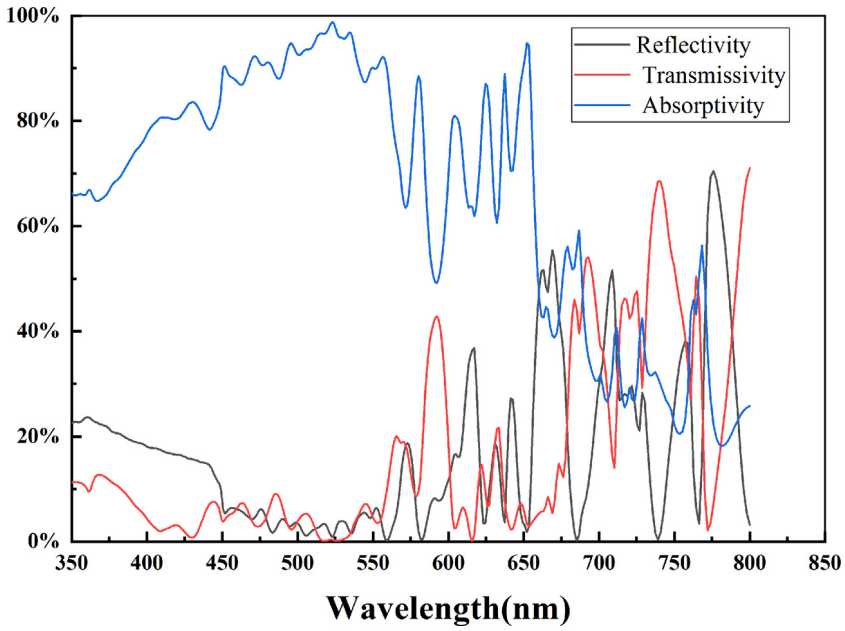


**Fig. 8.** Absorption, reflection, and transmission spectra of the green light PD. Black cure shows absorptivity, red cure shows transmissivity, blue cure shows reflectivity. . (For interpretation of the references to color in this figure legend, the reader is referred to the web version of this article.)

Understanding the effects of parameters such as the thickness of the PD, the period, and the fill factor of the micro-nano optical structure on the absorptivity will facilitate the design of an ideal device.

From the absorptivity cure of the blue PIN PD (Fig. 7), it can be seen that in the range of 400 nm $< \lambda <$ 550 nm, the absorptivity of the spectrum was very high, and the absorptivity curve was relatively smooth. This was because the channeling mode and fundamental mode exist simultaneously in this band. The channeling mode greatly reduces the reflectivity, thus improving absorptivity. When $\lambda >$ 600 nm, the waveform was sharp because of simultaneous existence of the fundamental mode and the guided resonance mode. For the green PD (Fig. 8), the absorptivity was very high at 450 nm $< \lambda <$ 650 nm, again due to the reduction of reflectivity by the channeling mode. As shown in the absorptivity spectrum for the red PD (Fig. 9), there was a steep wave peak at about 620 nm caused by the guided resonance mode. When the wavelength is greater than 600 nm the channeling mode is not the main mode, and if the absorption depth is larger than 1 μm, it can form absorption peaks using guided mode resonance. If the PD thickness is greater than the absorption depth, the absorptivity increases as a result of the decreased reflectivity caused by the channeling mode. If the thickness is less than the absorption depth, the absorptivity can be increased by the guided resonance mode.

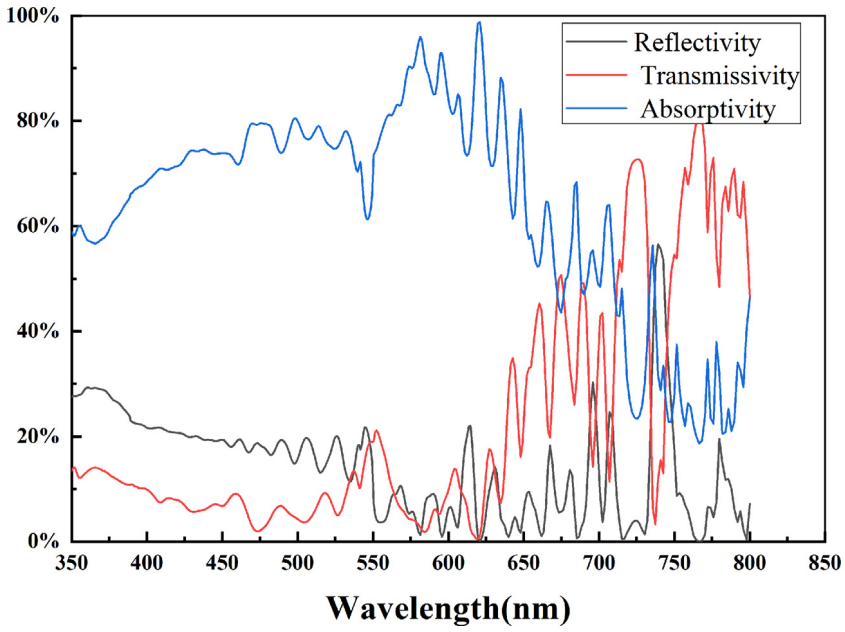


**Fig. 9.** Absorption, reflection, and transmission spectra of the red light PD. Black cure shows absorptivity, red cure shows transmissivity, blue cure shows reflectivity. . (For interpretation of the references to color in this figure legend, the reader is referred to the web version of this article.)

### *2.4. Process design*

The trichromatic light PDs were simultaneously included in one chip to improve the integration of the device. The specific process flow was as follows (as shown in Fig. 10).

1. An SOI chip with a top-silicon thickness of 1 μm was selected, and the silicon wafer of the SOI structure was placed in piranha solution, ethanol, acetone, ethanol, and deionized water for ultrasonic cleaning.

2. The protective layer was spin-coated onto the surface of the silicon wafer and then baked on a hot plate before photolithography, followed by removal of the redundant protective layer in the developer, and, finally, the hard film treatment on the hot plate.

3. The B-doped $p^{++}$ layer as the p-ohmic contact was formed by ion implantation, then the mask layer was removed.

4. The protective layer was patterned (step 2) and a P-doped n++ layer fabricated as the n-ohmic contact, followed by removal of the mask layer.

5. The protective layer was patterned (step 2), then the isolated part was formed by wet or dry etching, followed by removal of the mask layer.

6. The protective layer was patterned (step 2), 20 nm/100 nm of Pt/Al was deposited by electron beam evaporation on the ohmic contact layer. Then the metal was lifted off in acetone, followed by final annealing in $N_2$ ambient conditions.

7. The protective layer was patterned using reactive ion etching or deep reactive ion etching to fabricate micro-nano optical structures of the trichromatic PD intrinsic layer, followed by removal of the mask layer.

## 3. Quantum efficiency

The photoelectric conversion efficiency of photodiodes is usually measured by quantum efficiency, which is usually divided into internal quantum efficiency $\eta_0$ and external quantum efficiency (EQE) $\eta$ [31]: the internal quantum efficiency is the average number of free electron–hole pairs generated by an absorbed photon; while the external quantum efficiency is defined as the ratio of the photo generated electron–hole pairs collected by the photodiode to the number of photons incident on the photodiode. For optical signals with incident light energy higher than or equal to the band gap width of semiconductor materials, the internal quantum efficiency $\eta_0$ of most semiconductor materials can be considered as constant, close to 1. Part of the photo-generated carriers cannot be collected during the transport to the electrodes due to recombination. For photodiodes, the reflection of incident light on the upper surfaces of the device will reduce the effective light signal intensity. In conclusion, the distribution of photogenerated carriers in the device is as follows [32, 33]:

$$S(x) = \frac{\eta_0 (1-R)\alpha}{1 - R^2 \exp(-2\alpha t)} \left[\exp(-\alpha x) + R \exp(-2\alpha t) \exp(-\alpha x)\right] \tag{1}$$

Where $R$ is the reflectivity, and $\alpha$ is the absorption coefficient of bulk silicon, and $t$ is the thickness of the photodiode.

The external quantum efficiency is simply the integral of this function over the detector thickness:

$$\begin{aligned} \eta &= \int_0^t S(x)\, dx \\ &= \frac{\eta_0 (1-R)\left[1 - \exp(-\alpha t)\right]}{1 - R \exp(-\alpha t)} \end{aligned} \tag{2}$$

It can be concluded from Eq. (2) that the external quantum efficiency of the device is related to the reflectivity of the upper surface of the device, the absorption coefficient of the material, and the thickness of the photodiode. Reducing the reflectivity of incident light on the surface of the device and increasing the thickness of the absorption region of the device are common means to improve the external quantum efficiency, which usually meets the condition of $\alpha t >> 1$. Because the absorption coefficient is a material property, only increasing the thickness of the absorption region of the device cannot improve the quantum efficiency significantly, and the increase of the thickness of the absorption region will increase the overall volume of the device, and affect other performances of the device. In this paper, only blue photodiode array can satisfy the $\alpha t > 1$ condition, while the parameters of red and green photodiode arrays are $\alpha t < 1$. From the discussion part, it is concluded that the design of micro nano optical structure in the intrinsic region of photodiode can enhance the light propagation mode in the material, which not only effectively reduces the reflectivity of the device surface, but also increases the light propagation distance in the material, thereby enhancing the light absorptivity of the photodiode array. When the incident light intensity changes to

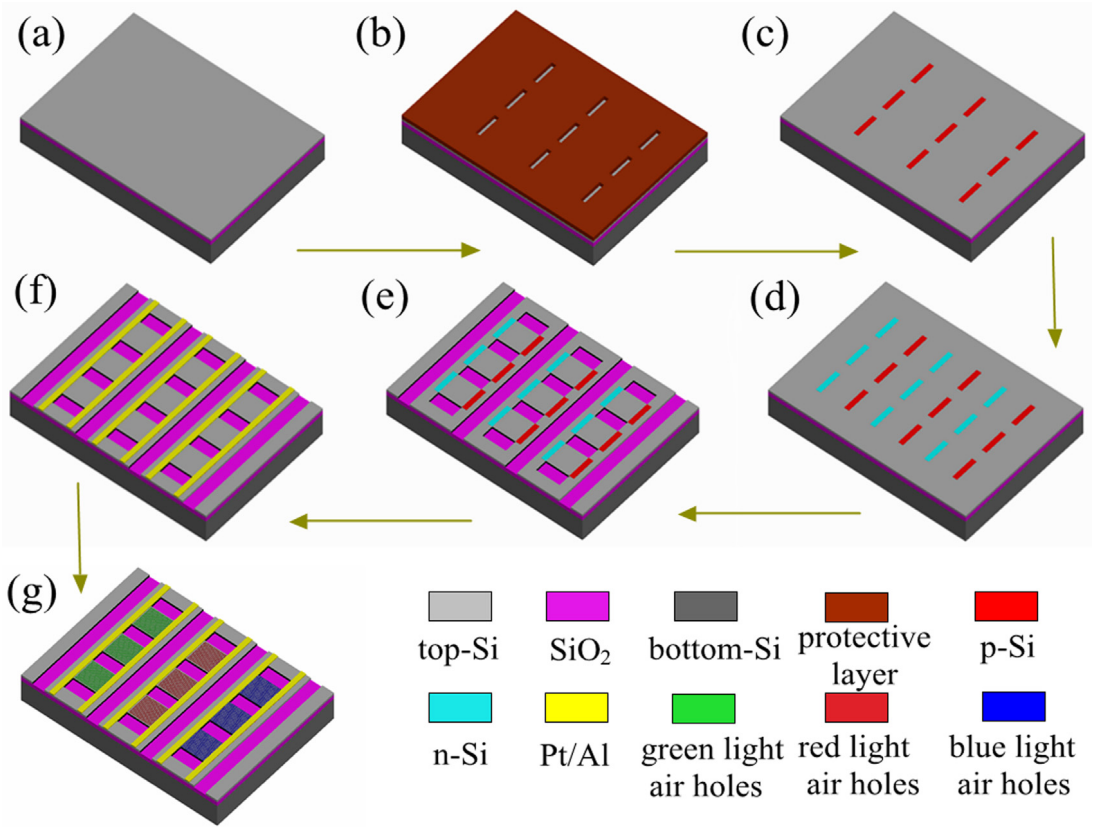


**Fig. 10.** Schematic illustration of the steps used in the fabrication of the ultra-thin lateral PIN trichromatic PD arrays. (a) Clean the chip. (b) Pattern the protective layer. (c) Form the p-Si layer by ion implantation. (d) Pattern the n-Si protective layer and fabricate the P-doped n++ layer. (e) Make the isolated part. The width of the isolation groove channel between the two pixels can be adjusted. By reducing the groove spacing, a guard ring can be formed to prevent breakdown. Increasing the groove spacing increases the heat dissipation. (f) Ohmic contact metallization. (g) Fabricate micro-nano optical structures in the trichromatic PD intrinsic layer.

**Table 2**
The effective absorption coefficient of blue light, green light and red light.

| Wavelength (nm) | $\alpha_{effective} = 1/s$ ($\mu m^{-1}$) | $\alpha$ ($\mu m^{-1}$) |
|---|---|---|
| 450 | 2.857142857 | 4.170131825 |
| 455 | 2.857142857 | 3.610075707 |
| 460 | 3.125 | 3.559102728 |
| 465 | 3.333333333 | 3.613505652 |
| 470 | 3.448275862 | 3.208434996 |
| 475 | 3.703703704 | 2.910106879 |
| 480 | 3.571428571 | 2.455797958 |
| 495 | 2.222222222 | 1.849485966 |
| 500 | 2.222222222 | 1.834690078 |
| 505 | 2.173913043 | 1.645596124 |
| 510 | 2.380952381 | 1.645596124 |
| 515 | 2.5 | 1.464043178 |
| 520 | 2.380952381 | 1.377467548 |
| 525 | 2.380952381 | 1.268605012 |
| 530 | 2.5 | 1.019535712 |
| 615 | 1.818181818 | 0.491193631 |
| 620 | 1.538461538 | 0.445903466 |
| 625 | 1.538461538 | 0.441629631 |
| 630 | 1.538461538 | 0.3989324 |
| 635 | 1.666666667 | 0.37600164 |
| 640 | 1.25 | 0.353982265 |
| 645 | 1.333333333 | 0.330693958 |
| 650 | 1.428571429 | 0.328658923 |

*1/e* of the initial value, the distance through which light passes is the absorption depth *s*. FDTD numerical simulation is used to obtain the absorption depth of three color photodiode arrays in blue (450 nm–480 nm), green (495 nm–530 nm) and red (615 nm–650 nm) bands, and the effective absorption coefficient $\alpha_{effective}$ is obtained (as shown in Table 2).

It can be summarized from Table 2 that the effective absorption coefficient of blue light is very similar to the absorption coefficient of bulk silicon, with little change, and the effective absorption coefficient of green light is twice higher than the absorption coefficient, and the effective absorption coefficient of red light is higher than the absorption coefficient Four times. This means that the thickness of the absorption region of the flat surface photodiode has to be increased by four times in order to have the same external quantum efficiency as the photodiode with micro-nano optical structure for red light.

The simulated absorptivity values depicted in Fig. 11 were compared with the theoretical EQE values, and the theoretical EQE values were similar to the simulated values of absorptivity for blue light, and the theoretical values were lower than the simulated values of absorptivity for green and red light. The EQE of micro-nano optical structure PD was much higher than the flat surface PD. At the blue light wavelength ($\lambda$ = 470 nm), a Si photodiode with a flat surface designed with an i-layer thickness of 1 μm will exhibit an EQE of only ~59.4%, but photodiodes with integrated holes exhibited ~95.1% EQE. At the green light wavelength ($\lambda$ = 525 nm), the EQE of the designed structure gets 88.9%, which is 74% higher than the value of the flat surface structure. At the red light wavelength ($\lambda$ = 620 nm), the EQE of the photodiode with micro-nano hole array in the intrinsic region is twice that of the unstructured photodiode. So the micro-nano optical structure not only can increase the absorptivity of the photodiode, but also can increase the EQE of the photodiode.

## 4. Response bandwidth

The capacitance of a silicon-based PIN photodetector primarily affects the charge–discharge time (rise time) of the device. An *RC* loop is formed by the capacitance of the silicon-based PIN photodetector and

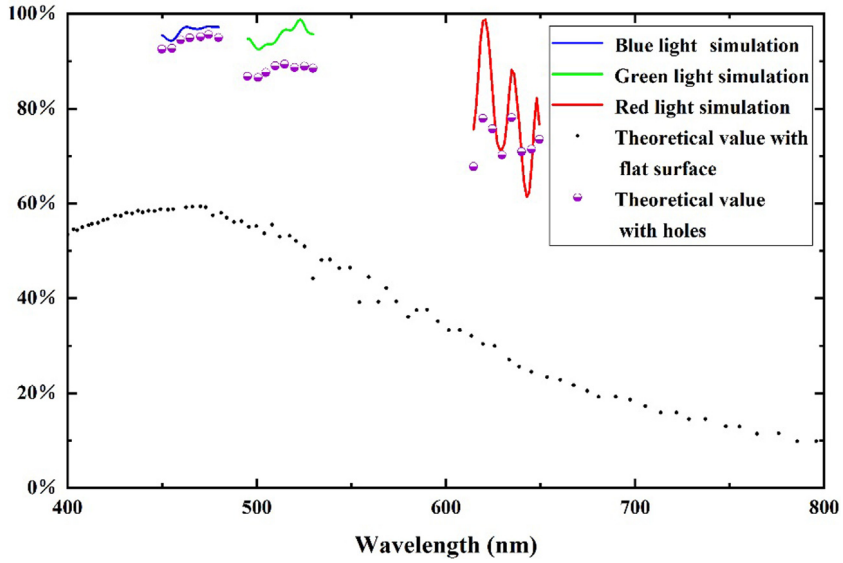


**Fig. 11.** The external quantum efficiency of the lateral PIN trichromatic PD arrays and flat surface PD. The blue, green, and red curves are the absorption rates of blue, green, and red photodiode arrays obtained by FDTD numerical simulation. The purple semi-solid circle is the theoretical external quantum efficiency of the three-color photodiode array, and the black solid point is the theoretical quantum efficiency of the flat surface photodiode. . (For interpretation of the references to color in this figure legend, the reader is referred to the web version of this article.)

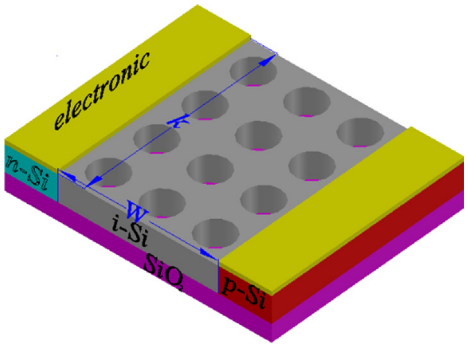


**Fig. 12.** A pixel of lateral PIN trichromatic PD arrays with micro-nano optical holes.

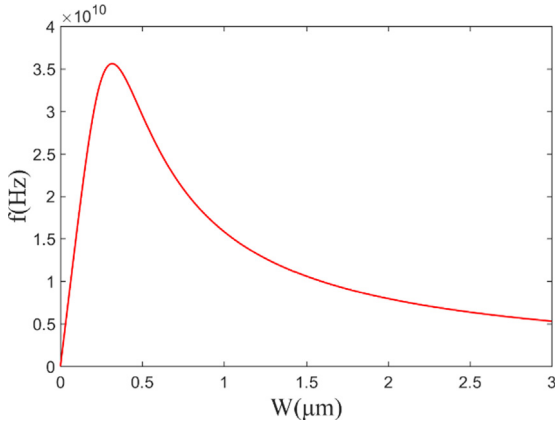


**Fig. 13.** Relationship between the response bandwidth $f$ and the thickness W of the intrinsic layer.

the series resistor. In a high-frequency working environment, when the rise time of the loop cannot keep up with the frequency change, the device cannot work normally; that is, the capacitance of the silicon-based PIN photodetector directly affects the response speed of the device via the rise time. According to the $RC$ time constant $\tau = R_L C$, the smaller the capacitance of the device, the shorter the rise time.

In an ideal PIN diode, the capacitance is defined as

$$C = \varepsilon \frac{A}{W}, \tag{3}$$

Where $A$ is the junction area ($A$=$k$*$t$), $\varepsilon$ is the semiconductor dielectric constant, and $W$ is the width of the depletion layer, which is composed of the i-layer (as shown in Fig. 12). Compared to the $n^{++}$ layer and the $p^{++}$ layer, the intrinsic layer is a high-resistance zone, so most of the applied reverse bias falls to the i-layer, which becomes a depletion layer completely.

In VLC, because the incident light intensity is modulated at a high frequency, the PD is required to respond to the corresponding changes quickly (i.e., bandwidth). The response bandwidth of a lateral PIN PD is affected by two main factors. (1) The drift time in the depletion layer, which is the major factor affecting the bandwidth. In order to reduce the transition time of the depletion layer, the depletion layer should be as narrow as possible, but too narrow a depletion layer will reduce the number of photons absorbed by the device, thus affecting the quantum efficiency. (2) The depletion layer capacitance. If the depletion layer is too narrow, the capacitance of the depletion layer will be too large, and so the time constant $\tau$ will be too large.

$$f_{3dB} \approx \frac{1}{2\pi\sqrt{t_r^2 + (R_L C)^2}} \tag{4}$$

In formula (2), $f_{3dB}$ is 3 dB frequency, where $t_r \approx W/v_s$ is the transition time of the depletion layer and $v_s$ is the saturation drift speed.

When the load resistance $R_L$ in the $RC$ loop is 1 kΩ, the width of a single pixel is 10 μm; according to formula (2), the relationship between the response bandwidth $f_{3dB}$ and the thickness $W$ of the intrinsic layer can be obtained as shown in Fig. 13.

It can be seen from Fig. 13, as the thickness of the absorber layer increases, the bandwidth also increases to a certain thickness and then decreases. When the thickness of the intrinsic layer of the device is within a certain range, the parasitic capacitance plays a leading part in the time response of the whole device. As the thickness increases, the parasitic capacitance decreases, and the response time is faster, and the bandwidth increases. When the thickness of the intrinsic layer continues to increase, the capacitance continues to decrease. However, the transport time of the carriers in the device increases significantly

and affects the time response characteristics; that is, the thickness of the intrinsic layer continues to increase and the effective time of carrier transport dominates the time response of the device, causing a time delay, which in turn reduces bandwidth.

Experiments have shown that the best choice for depletion layer width is [34]

$$2\pi f_{3dB} t_r = 2.4. \tag{5}$$

For the required cutoff frequency, the width of the depletion layer can be designed according to formula (3). Thus, when $f$ is 1–10 GHz, the depletion layer width $W$ is 4 to 40 μm.

When light irradiates the reverse-biased PD, the electron–hole pairs generated by the light separate in the depletion layer. Electrons move to the N-region and holes move to the P-region, thereby a current is created in the external circuit. When operating at high frequencies, the depletion layer must be thin to reduce the transit time and achieve high response speeds. At the same time, in order to increase quantum efficiency, the depletion layer must be thick enough to absorb most of the incident light. The response bandwidth and quantum efficiency are contradictory to the design of the device and need to be considered. Considering these factors, we set the depletion layer width to 10 μm.

When the depletion layer width is 10 μm, it can be concluded from formula (3) that the capacitance of a single pixel is 0.1 fF. And it can be seen from Fig. 11 that when the depletion layer width is larger than 3 μm, the time of drift in the depletion layer dominates, so when the depletion layer width is 10 μm, the response bandwidth is determined by $t_r$, that is, 1.6 GHz.

## 5. Conclusion

In this work, a lateral PIN PD structure based on SOI was used to increase the light incident area. A new ultra-thin trichromatic PIN PD array with micro-nano optical structure was designed. This structure could enhance the PD absorptivity of blue, green and red light. At the central wavelength of blue light, the light absorptivity reached 96.8%, and the EQE reached 95.1%. When the wavelength $\lambda$ was in the range of 450–480 nm, the absorptivity was greater than 94%. The absorptivity at the center of the green light reached 97.5%, and the EQE reached 88.9%, and the absorptivity was greater than 92% in the range of $\lambda$ from 495 nm to 530 nm. The absorptivity at the center of the red light reached 98.6%, and the EQE reached 77.9%, and the absorptivity was greater than 61% in the range of $\lambda$ from 615 nm to 650 nm. The structure of the PD designed in this study could also improve the response bandwidth of the device. When the depletion layer width was 10 μm, the capacitance of a single pixel was 0.1 fF and the response bandwidth was 1.6 GHz.

## Declaration of competing interest

The authors declare that they have no known competing financial interests or personal relationships that could have appeared to influence the work reported in this paper.

## Acknowledgments

This work was supported in parts by Science and technology projects of Guangdong Province (Grant Nos. 2015B010125007, 2016B010111003); National Key Research and Development Project (No. 2018YFB1801900); Project of Guangzhou Industry Leading Talents (CXLJTD-201607).

## References

[1] D. O'Brien, H.L. Minh, L. Zeng, G. Faulkner, K. Lee, D. Jung, Y. Oh, E.T. Won, Indoor visible light communications: challenges and prospects, Proc. SPIE 7091 (2008) 709106.
[2] Y. Wang, Y. Wang, N. Chi, J. Yu, H. Shang, Demonstration of 575-Mb/s downlink and 225-Mb/s uplink bi-directional SCM-WDM visible light communication using RGB LED and phosphor-based LED, Opt. Express 1 (21) (2013) 1203–1208.
[3] Y. Wang, X. Huang, L. Tao, J. Shi, N. Chi, 4.5-Gb/s RGB-LED based WDM visible light communication system employing CAP modulation and RLS based adaptive equalization, Opt. Express 23 (10) (2015) 13626–13633.
[4] Y. Wang, Y. Wang, N. Chi, J. Yu, H. Shang, Demonstration of 575-Mb/s downlink and 225-Mb/s uplink bi-directional SCM-wdm visible light communication using RGB LED and phosphor-based LED, Opt. Express 21 (1) (2013) 1203–1208.
[5] D. Tsonev, H. Chun, S. Rajbhandari, J. McKendry, S. Videv, E. Gu, M. Haji, S. Watson, A. Kelly, G. Faulkner, M. Dawson, H. Haas, D. O'Brien, A 3-Gb/s single-LED OFDM-Based wireless VLC link using a gallium nitride $\mu$LED, IEEE Photon Technol. Lett. 26 (7) (2014) 637–640.
[6] A. Afzalian, D. Flandre, Physical modeling and design of thin-film SOI lateral PIN photodiodes, IEEE Trans. Electron. Dev. 52 (6) (2005) 1116–1122.
[7] A. Afzalian, D. Flandre, Monolithically integrated 10Gb/s photodiode and transimpedance amplifier in thin-film SOI CMOS technology, IEEE Electron. Lett. 42 (24) (2006) 1420–1421.
[8] A. Afzalian, D. Flandre, Seed performances of thin-film lateral SOI PIN photodiodes up to tens of GHz, in: Proceedings of the IEEE International SOI Conference, 2006, pp. 83–84.
[9] A. Afzalian, D. Flandre, Measurements, modeling and electrical simulations of lateral PIN photodiodes in thin film-SOI for high quantum efficiency and high selectivity in the UV range, in: Proceedings of the ESSDERC Conference, Estoril, Portugal, 2003, pp. 55–58.
[10] A. Afzalian, D. Flandre, Characterization of quantum efficiency, effective lifetime and mobility in thin film ungated SOI lateral PIN photodiodes, Solid State Electron. 51 (2) (2007) 337–342.
[11] Y. Gao, H. Cansizoglu, K.G. Polat, S. Ghandiparsi, A. Kaya, H.H. Mamtaz, A.S. Mayet, Y. Wang, X. Zhang, T. Yamada, E. Ponizovskaya Devine, A.F. Elrefaie, S.-Y. Wang, M.S. Islam, Photo-trapping microstructures enable high-speed high-efficiency silicon photodiodes, Nature Photon. 5 (11) (2017) 301–308.
[12] T. Ishi, J. Fujikata, K. Makita, T. Baba, K. Ohashi, Si nano-photodiode with a surface plasmon antenna, Japan. J. Appl. Phys. 44 (2005) L364.
[13] R.T. Chen, Lei Lin, Chulchae Choi, Y.J. Liu, B. Bihari, L. Wu, S. Tang, R. Wickman, B. Picor, M.K. Hibb-Brenner, J. Bristow, Y.S. Liu, Fully embedded board-level guided-wave optoelectronic interconnects, Proc. IEEE 88 (2000) 780–793.
[14] Y. Kang, et al., Monolithic germanium/silicon avalanche photodiodes with 340 GHz gain-bandwidth product, Nature Photon. 3 (2009) 59–63.
[15] W. Huang, Y. Liu, Y. Hsin, A high-speed and high-responsivity photodiode in standard CMOS technology, IEEE Photon. Technol. Lett. 19 (2007) 197–199.
[16] S. Assefa, F. Xia, Y.A. Vlasov, Reinventing germanium avalanche photodetector for nanophotonic on-chip optical interconnects, Nature 464 (2010) 80–84.
[17] M. Atef, A. Polzer, H. Zimmermann, Avalanche double photodiode in 40 nm standard CMOS technology, IEEE J. Quantum Electron. 49 (2013) 350–356.
[18] S. Csutak, J. Schaub, S. Wang, J. Mogab, J. Campbell, Integrated silicon optical receiver with avalanche photodiode, IEEE Proc. Optoelectron. 150 (2003) 235–237.
[19] P. Kumar, et al., Experimental Aspects of Quantum Computing, Springer, 2005, pp. 215–231.
[20] H.C. Yuan, et al., Flexible photodetectors on plastic substrates by use of printing transferred single-crystal germanium membranes, Appl. Phys. Lett. 94 (2009) 013102.
[21] E. Garnett, P.D. Yang, Light trapping in silicon nanowire solar cells, Nano Lett. 10 (2010) 1082–1087.
[22] M.D. Kelzenberg, et al., Enhanced absorption and carrier collection in Si wire arrays for photovoltaic applications, Nature Mater. 9 (2010) 239–244.
[23] A. Zhang, H. Kim, J. Cheng, Y.H. Lo, Ultrahigh responsivity visible and infrared detection using silicon nanowire phototransistors, Nano Lett. 10 (2010) 2117–2120.
[24] Y. Park, et al., Absorption enhancement using photonic crystals for silicon thin film solar cells, Opt. Express 17 (2009) 14312–14321.
[25] H. Shigeta, et al., Enhancement of photocurrent in ultrathin active-layer photodetecting devices with photonic crystals, Appl. Phys. Lett. 101 (2012) 161103.
[26] K.X.Z. Wang, et al., Light trapping in photonic crystals, Energy Environ. Sci. 7 (2014) 2725–2738.
[27] S.E. Han, G. Chen, Optical absorption enhancement in silicon nanohole arrays for solar photovoltaics, Nano Lett. 10 (2010) 1012–1015.
[28] T. Fuse, M. Ohta, M. Tokumasu, et al., A 0.5V Power-supply scheme for low-power system LSIs using multi-Vth SOI CMOS technology, IEEE J. Solid-State Circuits 38 (2) (2003) 303–311.
[29] B.C.P. Sturmberg, K.B. Dossou, L.C. Botten, A.A. Asatryan, C.G. Poulton, C.M. de Sterke, R.C. McPhedran, Modal analysis of enhanced absorption in silicon nanowire arrays, Opt. Express 19 (2011) 1064–1081.

[30] Justin L. Donnelly, Bjrn C.P. Sturmberg, Kokou B. Dossou, Lindsay C. Botten, Ara A. Asatryan, Christopher G. Poulton, Ross C. McPhedran, C. Martijn de Sterke, Mode-based analysis of silicon nanohole arrays for photovoltaic applications, Opt. Express 22 (2014) A1343–A1354.
[31] Jinzhong Yu, Semiconductor Optoelectronic Technology, Chemical Industry Press, Beijing, 2003, pp. 58–138.
[32] Richard D. Nelson, Infrared charge transfer devices: The silicon approach, Optic. Eng. 16 (3) (1977) 163275.
[33] M. Razeghi, A. Rogalski, Semiconductor ultraviolet detectors, Appl. Phys. Rev. 75 (10) (1996) 7433–7473.
[34] Qingju Meng, Haibo Liu, Qinghui Meng, Semiconductor Device Physics, vol. 11, Science Press, Beijing, 2009, chap 8:269.